Chaos ARTICLE scitation.org/journal/cha

Front propagation steered by a high-wavenumber modulation: Theory and experiments

Cite as: Chaos **30**, 053138 (2020); doi: 10.1063/5.0003519
Submitted: 2 February 2020 · Accepted: 4 May 2020 ·
Published Online: 26 May 2020

K. Alfaro-Bittner,[1,a)] C. Castillo-Pinto,[2] M. G. Clerc,[2] G. González-Cortés,[2] G. Jara-Schulz,[2] and R. G. Rojas[3]

AFFILIATIONS

[1]Departamento de Física, Universidad Técnica Federico Santa María, Av. España 1680, Casilla 110V, Valparaíso, Chile
[2]Departamento de Física and Millennium Institute for Research in Optics, FCFM, Universidad de Chile, Casilla 487-3, Santiago, Chile
[3]Instituto de Física, Pontificia Universidad Católica de Valparaíso, Casilla 4059, Valparaíso, Chile

Note: This article is part of the Focus Issue, instabilities and Nonequilibrium Structures.
[a)]**Author to whom correspondence should be addressed:** karin.alfaro@usm.cl

ABSTRACT

Homogeneously driven dynamical systems exhibit multistability. Depending on the initial conditions, fronts present a rich dynamical behavior between equilibria. Qualitatively, this phenomenology is persistent under spatially modulated forcing. However, the understanding of equilibria and front dynamics organization is not fully established. Here, we investigate these phenomena in the high-wavenumber limit. Based on a model that describes the reorientation transition of a liquid crystal light valve with spatially modulated optical forcing and the homogenization method, equilibria and fronts as a function of forcing parameters are studied. The forcing induces patterns coexisting with the uniform state in regions where the system without forcing is monostable. The front dynamics is characterized theoretically and numerically. Experimental results verify these phenomena and the law describing bistability, showing quite good agreement.

Systems driven by homogeneous energy injection are characterized by exhibiting dissipative equilibria, i.e., attractors. Inhomogeneous initial conditions lead to the formation of different domains. Walls or fronts separate these domains. These fronts show a rich complex spatiotemporal dynamics such as those observed in the spread of fires, crystal growth, disease propagation, and explosions. These phenomena are persistent when the systems are forced with spatially modulated energy injection. In this context, patterns replace the homogeneous states. The front dynamics between patterns and homogeneous states are characterized by a hopping dynamics, viz., fronts are propagated by means of abrupt jumps. Analytical understanding of equilibria organization and the front dynamics is an open question. To address this issue, the high-wavenumber modulation limit and homogenization method are considered. Then, equations with inhomogeneous coefficients are transformed into effective equations with homogeneous coefficients. Hence, analytical analyses are accessible. Here, we consider a liquid crystal light valve with optically modulated forcing, which exhibits multistability and fronts between these states. Due to the competition between electrical and elastic force, the liquid crystals present a transition. Close to this instability, an amplitude equation allows us to elucidate that the forcing induces coexistence between patterns and a uniform state in regions where the system without forcing is monostable. Likewise, this model allows front dynamics characterization. Experimental observations are in good agreement with theoretical findings.

I. INTRODUCTION

Out of equilibrium systems are characterized by a permanent injection of energy, momentum, or particles.[1–4] Changing the physical parameters, these systems exhibit coexistence between different equilibria as a result of spontaneous breaking symmetries. Due to the inherent fluctuations of macroscopic systems, these transitions are characterized by the emergence of different domains.[3,4] A domain corresponds to a spatial region where an equilibrium manifests itself. Different states are separated by domain walls. Depending on the context, these domain walls are usually called

interfaces, grain borders, and fronts, among others.[5–16] Interfaces can be observed in different spatial dimensions, even in one spatial dimension.[14,16] From dynamical systems point of view, fronts correspond to heteroclinic curves in a co-mobile system.[17] Indeed, domain walls are solutions connecting two equilibria of a given system.

These fronts dynamics depend on the relative stability between equilibria. In variational or gradient systems, the speed of front propagation between two uniform stable states, *bistable fronts*, is proportional to the energy difference,[6] where a lower energy state invades an upper energy state. Even if the state of lower energy is unstable (half-stable), it can invade a stable state of higher energy.[18] Hence, bistable fronts are characterized by being motionless for a single value of a parameter, *the Maxwell point*.[4] The above description remains valid for the non-variational systems.[19] The main difference is that the front propagation mechanism in the non-variational case is still an open question. Even when the front connects two symmetric states, it can propagate as a result of spontaneous parity symmetry breaking. This phenomenon is well-known as non-variational Ising–Bloch mechanism.[20–22]

The previous scenario changes drastically when the front connects a stable state with an unstable one.[8,11,23–30] These types of fronts are usually called FKPP fronts, in honor of the pioneering works of Fisher[23] and Kolmogorov *et al.*[24] The speed of front propagation into an unstable state depends on the initial conditions. As a matter of fact, if one considers a bounded disturbance of the unstable state, it always spreads with minimum speed. This speed either depends on the linearization around the unstable state (pulled front) or on the nonlinear dynamics (pushed front).[11] FKPP fronts have been reported in fluid dynamics,[25,26] phase transitions,[27] liquid crystal light valves with optical feedback,[28–30] fiber optics resonators,[31–33] and population dynamics.[8]

Likewise, when one considers a front between a homogeneous state and a periodic structure or between pattern states in one spatial dimension, the propagation speed exhibits utterly different behavior. As a result of the spatial translation breaking symmetry induced by the pattern state, the front is motionless in a range of parameters independent of the relative stability between equilibria.[6] This phenomenon is known in the literature as the *pinning effect*. The origin of this effect is the induction of a nucleation barrier in the front position dynamics.[34] Experimental verification of this phenomenon has been achieved in liquid crystal light valves with spatially modulated optical feedback[14] and in a delayed bistable semiconductor laser with optoelectronic feedback.[35] Reference 14 shows that a bistable regime with spatially modulated forcing exhibits coexistence of patterns. Close to the reorientation instability of the liquid crystal, the system exhibits bistability between a uniform state and an induced pattern.[29] The wavelength of the pattern is imposed by the spatial forcing. The characteristic scale of fronts connecting two homogeneous states is the length of the transition region between equilibria, which is usually called the front core. Figure 1 depicts the front core by symbol l. Based on the separation of spatial scales theory, *homogenization*,[36–39] one expects the fronts dynamics to be analytically accessible and understandable.

This paper aims to investigate fronts dynamics steered by a with high-wavenumber forcing. Theoretically, a model describing the reorientation instability of a liquid crystal light valve subjected to a spatially modulated optical forcing, which corresponds to a scalar spatial forcing model with cubic-quintic nonlinearity, is considered. Based on spatial homogenization methods valid at the high-wavenumber limit, the equilibria as a function of forcing parameters are studied. Spatial forcing induces patterns coexisting with the uniform state in regions where the unforced system is monostable, namely, the spatial forcing causes bistability. Analytically, we establish the bistability regions as a function of the wavenumber. The proposed law has been experimentally verified finding quite good agreement with theoretical predictions. Fronts connecting uniform and pattern states have been observed in a bistable region. Also, a continuous transition from bistable to FKPP fronts is observed as a function of the bifurcation parameter. First corrections in the fast scale of the homogenized equation allow the characterization of fronts and their propagation speed. Pinning region and front speed can be predicted due to these corrections. All described phenomena have been experimentally observed, presenting qualitatively good agreement with the theoretical findings.

II. BISTABLE MODEL WITH SPATIAL MODULATION FORCING

Liquid crystal cells with photosensitive walls and spatial modulated optical feedback exhibit a subcritical transition, which is described by the dimensionless bistable model (see Refs. 10 and 29 for details),

$$\partial_t u(x,t) = [\mu + \gamma \sin(kx)]u + \beta u^2 + \alpha u^3 - u^5 + \partial_{xx} u, \quad (1)$$

where $u(x,t)$ accounts for the critical elastic mode amplitude of a planar liquid crystal cell molecular reorientation subjected to an orthogonal electric field. x and t account for the transverse coordinate and time. μ is the bifurcation parameter which is proportional to the difference between the applied voltage and Fréedericksz voltage. Indeed, $\mu = 0$ corresponds to the reorientational transition point. γ and k account for the strength amplitude and the wavenumber of the spatial optical forcing, respectively. β is a phenomenological parameter which stands for the pretilt generated by the anchoring condition in the sample walls. The cubic and quintic terms account for the nonlinear elastic and electric response of the liquid crystal light valve with optical feedback.[10] The nonlinear response is controlled by the α parameter, which is a function of the elastic constants, dielectric susceptibility, and the intensity of the electric field. The last term accounts for the elastic coupling of the liquid crystal. Physically, the amplitude should be a positive defined quantity, i.e., $u(x,t) \geqslant 0$.

A. Unforced reorientational transition

When the optical forcing is homogeneous, the system is not spatially forced, $\gamma = 0$. Figure 1(a) shows the bifurcation diagram of an unforced system, the total intensity of amplitude $||u(x,t)|| = \int u(x,t)dx$ vs the bifurcation parameter μ. The trivial state of this system corresponds to the planar state $u = 0$. This state is stable (unstable) for $\mu \leqslant 0$ ($\mu > 0$). The other homogeneous states u_s satisfy the relationship $\mu + \beta u_s + \alpha u_s^2 - u_s^4 = 0$. Continuous and dashed non-horizontal curves account for the stationary solutions

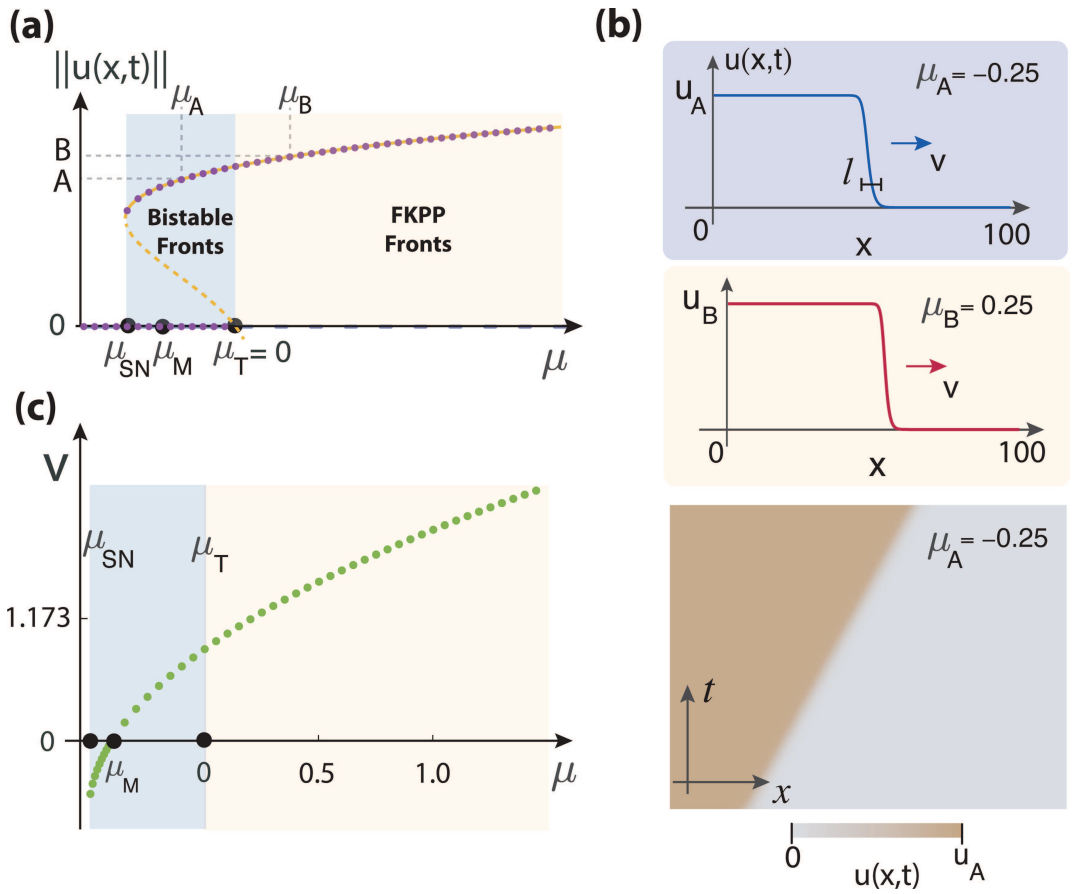

FIG. 1. Front solutions of unforced bistable model equation (1) by $\beta = 0.5$, $\alpha = 0.8$, and $\gamma = 0$. (a) Bifurcation diagram of unforced bistable model equation (1), the total intensity of amplitude $||u(x,t)|| = \int u(x,t)\,dx$ vs bifurcation parameter μ. Continuous and dashed curves account for stable and unstable states, respectively. Points account for homogeneous states obtained by numerical simulations of Eq. (1). The left (white), middle (blue), and right (yellow) painted areas show, respectively, the monostable, bistable, and coexistence regions. The symbols $A = 102.4$ and $B = 118.2$ account for some typical values of the total intensity of amplitude. μ_T, μ_{SN}, and μ_M account for the bifurcation, bistable, and Maxwell point, respectively. (b) Profile and spatiotemporal diagram of fronts between planar ($u = 0$) and reorientation state ($u > 0$), in the region of bistability and coexistence. The value of the reorientation state is represented by $u_A = 1.024$ and $u_B = 1.182$, respectively. l accounts for the size of the front core. (c) Front speed V as a function of the bifurcation parameter μ. The points stand for the front speed obtained by numerical simulations.

in Fig. 1. Experimentally, the β parameter is very small; in this limit, the stable and unstable states have the explicit expressions $u_s^s = (\alpha + \sqrt{\alpha^2 + 4\mu})/2$ and $u_s^u = (\alpha - \sqrt{\alpha^2 + 4\mu})/2$, respectively. Hence, the system exhibits bistability for $-\alpha^2/4 \leqslant \mu \leqslant 0$ and is monostable for $\mu > 0$. The previous bifurcation corresponds to a subcritical bifurcation, which is characterized by three critical points, the transition ($\mu_T = 0$), the emergence of bistability (μ_{SN}), and the Maxwell point (μ_M). Indeed, the critical points μ_{SN} and μ_T characterize the limits of the bistability region. The Maxwell point μ_M corresponds to the location in the parameter space, where the relative stability of the equilibria is the same.

The left (white), middle (blue), and right (yellow) areas show, respectively, the monostable, bistable, and coexistence regions in Fig. 1(a). In both regions (blue and yellow areas), the system presents coexistence between the planar ($u = 0$) and the reoriented state (u_s^s). Hence, it is expected to observe bistable and FKPP fronts. Figure 1(b) illustrates the typical front profile and spatiotemporal evolution. Note that the front spreads rigidly with a well-defined propagation speed. In fact, in the spatiotemporal diagram, one can draw a perfectly straight line of propagation. Figure 1(c) summarizes the front speed in the different regions. The front speed grows monotonously with the bifurcation parameter; for $\mu_{SN} < \mu < \mu_M$, the planar state invades the reoriented one. The above scenario is reversed when $\mu > \mu_M$. The front is motionless at $\mu = \mu_M$. For $\mu > \mu_T$, the front propagates into an unstable state and experimentally was studied in Ref. 29.

B. Reorientational transition with spatial modulation forcing

When the optical modulation forcing is considered ($\gamma \neq 0$), the system dynamics changes radically. As a result of spatial forcing, the uniform reoriented state becomes a spatially modulated state, i.e., a pattern (cf. Fig. 2). Hence, the system presents coexistence between a uniform equilibrium (planar state) and a pattern (reoriented state). Figure 2(a) shows the bifurcation diagram of the forced system. Note that the bistability region moves to the left flank. Therefore, the forcing induces that the spatially modulated state exists in the region that was initially monostable. Note that the bistable and transition point move a Δ and δ distance, respectively.

To shed light on the origin of the adaptation phenomenon between the bistability region and the front dynamics, the high-wavenumber modulation limit ($k \to \infty$) will be considered. In this limit, the rapid $x \sim k^{-1}$ and slow $Z \gg k^{-1}$ variation scales should be introduced. Considering the following ansatz for the amplitude of the critical mode:[36–39]

$$u = \phi(t, Z) + y(t, x, Z), \tag{2}$$

where the scalar field $\phi(t, Z)$ accounts for the slow dynamics of critical amplitude when one averages over the rapid spatial oscillation, *homogenized field*, that is,

$$\phi(t, Z) \equiv \lim_{k\to\infty} \frac{k}{2\pi} \int_{Z}^{Z+2\pi/k} u(x, t)\, dx. \tag{3}$$

The scalar field $y(t, x, Z)$ stands for small corrections of the homogenized field associated with rapid dynamics, that is, $y \ll 1$ and $\partial_{xx} y \gg l\partial_x y \gg l^2 y$, where l is the size of the front core. Introducing the previous ansatz in Eq. (1) and taking the dominant terms, we get

$$\partial_t \phi + \partial_t y \approx [\mu + \gamma \sin(kx)](\phi + y) + \beta\phi^2 + \alpha\phi^3 - \phi^5 + \partial_{xx}\phi + \partial_{xx} y. \tag{4}$$

Due to the separation of scales, the dominant term of the rapid dynamics is $\partial_{xx} y + \gamma \sin(kx)\phi = 0$. Integrating the previous equation, we have

$$y = \frac{\gamma}{k^2} \sin(kx)\phi + O\left(k^{-3}\right). \tag{5}$$

Replacing this expression in Eq. (4) and integrating it over a $2\pi/k$ period, after straightforward calculations, we obtain (the homogenized bistable model)

$$\partial_t \phi = \left[\mu + \frac{\gamma^2}{2k^2}\right]\phi + \beta\phi^2 + \alpha\phi^3 - \phi^5 + \partial_{ZZ}\phi. \tag{6}$$

Hence, in the limit of the high-wavenumber modulation, the homogenized field dynamics is derived, satisfying the unforced bistable equation (1) with a renormalized bifurcation parameter $\mu_F \equiv \mu + \gamma^2/2k^2$. Then, the bifurcation diagram of this model is similar to the unforced model but shifted in $\delta \equiv -\gamma^2/2k^2$. Indeed, the reorientation transition from planar to spatially modulated state occurs at $\mu_T = -\gamma^2/2k^2$. The critical amplitude mode is related

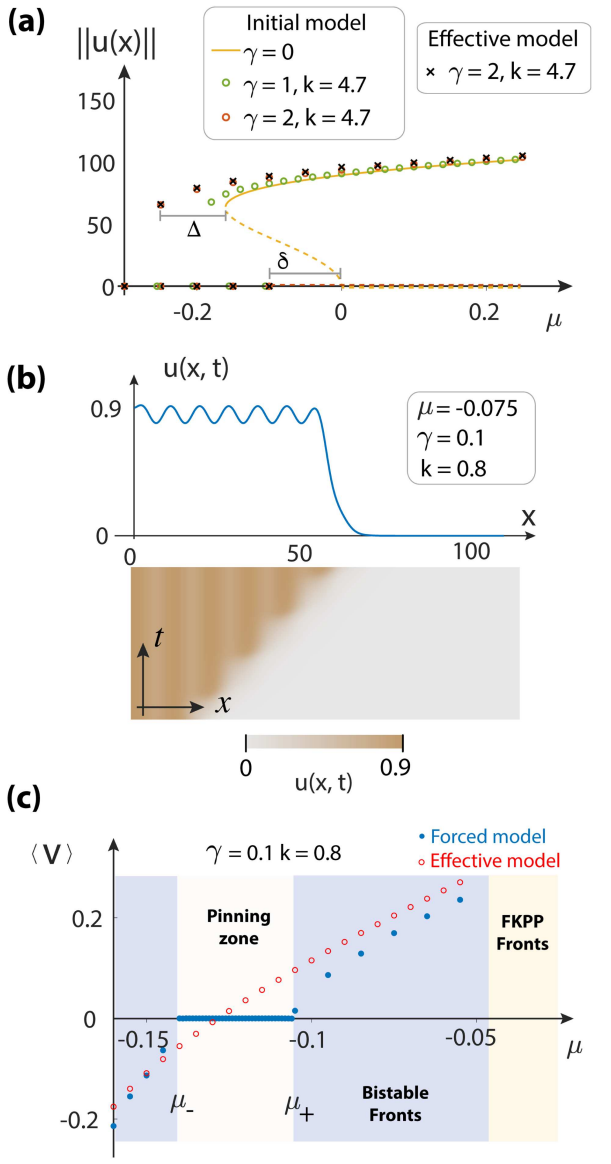

FIG. 2. Front solutions of the forced bistable model equation (1) for $\beta = 0.5$ and $\alpha = 0.8$. (a) Bifurcation diagram of the forced bistable model equation (1), the total intensity of amplitude $||u(x, t)||$ vs bifurcation parameter μ for $\gamma = \{0, 1, 2\}$ and modulation wavenumber $k = 4.7$. Continuous and dashed curves account for stable and unstable states, respectively. Points account for homogeneous states (patterns and uniform solution) obtained by numerical simulations of Eq. (1). The crosses (×) are obtained analytically from model equation (6). δ and Δ account for the displacement of the transition and bistable point, respectively. (b) Profile and spatiotemporal diagram of fronts between planar and spatial modulated reorientation state in the region of bistability. (c) Average front speed as a function of the bifurcation parameter. The blue (•) and red (○) dots stand for the front speed obtained by numerical simulations of model equations (1) and (6), respectively. The pinning region is given by $\mu_- < \mu < \mu_+$.

with homogenized field by

$$u \approx \left(1 + \frac{\gamma}{k^2}\sin(kx)\right)\phi. \tag{7}$$

Consequently, the zero state of ϕ corresponds to the planar state of the scalar field u. However, the non-zero homogeneous states correspond to spatial periodic wavelength solutions. Figure 2(a) shows the bifurcation diagram of the forced equation (1). This bifurcation diagram has quite good agreement with the induced by the homogenized field, which simply corresponds to a rigid translation of the bifurcation diagram. Therefore, the forcing induces patterns, which coexist with the planar state in a region where the unforced system is monostable. That is, the spatial forcing causes bistability, and when the wavenumber is increased, this region shrinks. Besides, when the strength γ increases, the bistability region grows. Figure 3 summarizes how the bistability region is modified when the forcing parameters are changed. Numerical simulations find excellent agreement using the formula $\mu_F = \mu + \gamma^2/2k^2 = 0$ and $\delta \equiv -\gamma^2/2k^2$. Note that the displacement of the critical transition and bistable point depends on the square of the optical modulation strength γ, this law is not valid for large γ. Furthermore, the numerical fitting of the critical point $\mu_T(k)$ as a function of the wavenumber shows excellent agreement [see Fig. 3(c)] with the theoretical prediction.

From the homogenized bistable model equation (6), is infered that the system has bistability and coexistence of equilibria. Thus, front solutions between the spatial modulated and planar state are expected. Figure 2(b) shows the profile and spatiotemporal evolution of the fronts between the zero state and the pattern in the bistability region. Note that as a consequence of the periodic spatial state, the front exhibits abrupt jumps, hopping dynamics.[34] The envelope of this oscillatory behavior is well defined by an average speed $\langle V \rangle$. Figure 2(c) displays the average front speed as a function of the bifurcation parameter μ. For negative and large bifurcation parameter, the planar state invades the reoriented one. Increasing this parameter results in a decrease in the average propagation rate. For a critical value $\mu = \mu_-$, the front becomes motionless. This dynamical behavior remains, while the bifurcation parameter satisfies $\mu_- < \mu < \mu_+$, the pinning region. For $\mu > \mu_+$, the front begins to spread so that the reoriented state invade the planar one. By increasing the bifurcation parameter, the front increases its average speed of propagation.

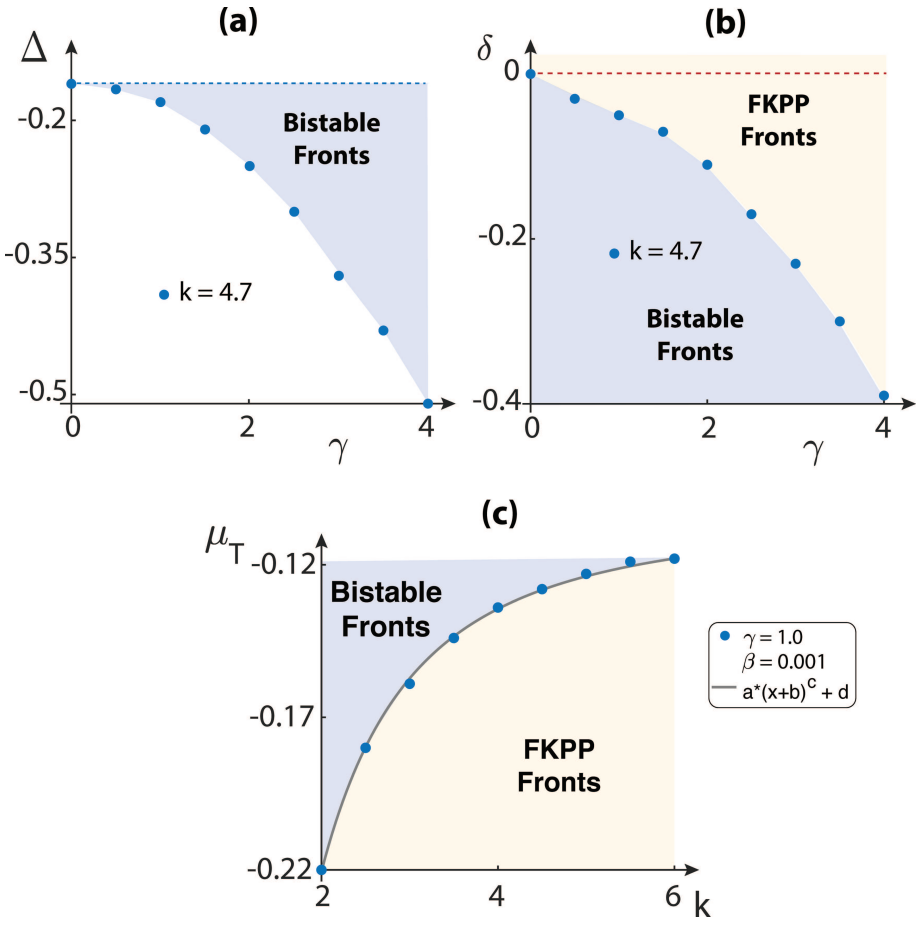

FIG. 3. Modification of the critical points as a function of forcing parameters. Modification of the bistability point Δ (a) and transition point δ (b) as a function of the optical modulated forcing strength γ for a fixed wavenumber k. The points are obtained by numerical simulation of the forced equation (1). (c) Transition point as a function of the wavenumber. The painted regions account for the region of bistability, coexistence, and monostability. The fitting curve considers $a = -0.51$, $b = 0.076$, $c = -2$, and $d = -0.1$.

III. FRONT PROPAGATION DYNAMICS IN SPATIALLY MODULATED FORCING SYSTEM

The limit of high-wavenumber modulation allows us to explain the equilibria organization and the possibility of having different front solutions. Indeed, in this limit, either spatially modulated uniform states are represented by uniform equilibria in the homogenized model [cf. Eq. (6)]. The front propagation is a consequence of the lower energy stable state invades the higher energy stable one.

The front is motionless only in the Maxwell point (cf. Fig. 1). Notwithstanding, Fig. 2(b) shows the front spatiotemporal evolution of spatially modulated model equation (1), which is characterized by a hopping dynamics. In addition, fronts are motionless in a range of bifurcation parameter [see Fig. 2(c)].

In brief, the homogenization approach does not account for the dynamics of fronts between the planar and the modulated reoriented state. Note that in this limit of separation of scales, it is well-known that the averaged equations do not correctly give the observed front dynamics, phenomenon known as a *non-resonant effect*.[6] To properly account for the dynamics, the amplitude equation must be amended.[14,34] Namely, the terms that have been neglected in the homogenization procedure must be considered, accounting the coupling between different scales. Calculating more precisely the integrals using the Laplace integral or stationary phase approximation,[40] one obtains the following averaged equation ($k \gg 1$):

$$\partial_t\phi = \left[\mu + \frac{\gamma^2}{2k^2}\right]\phi + \beta\phi^2 + \alpha\phi^3 - \phi^5 + \partial_{ZZ}\phi - \frac{\gamma\cos(kz)\partial_z\phi}{k^3}\left[\mu + 4\beta\phi + 9\alpha\phi^2 + 25\phi^4 + \gamma\sin(kz)\right]. \tag{8}$$

Note that Eqs. (1) and (8) are forced bistable systems. However, in the limit of large wavenumber, the forcing terms of Eq. (8) are of a perturbative nature. Numerical simulations of model equation (8) show that the front speed has a similar behavior of the forced system equation (1). Thus, depending on the parameters, fronts can propagate with hopping dynamics or be motionless.

Close to the Maxwell point, $\mu_M = -3\alpha^2/16 - \gamma^2/2k^2$, the amended model equation (8) has a motionless front solutions of the form

$$\phi_F(z, z_0) = \sqrt{\frac{3/4}{1 + e^{\pm\sqrt{3/4}\alpha(z-z_0)}}}, \tag{9}$$

where z_0 parametrizes the front position. Note that this stationary solution connects the planar state ($\phi = 0$) with the reoriented one ($\phi = \sqrt{3/4}$). In order to determine the effect of the amended terms, we can consider the following ansatz for the front (method of parameter variations):

$$\phi = \phi_F(z - z_0(t)) + w(z, z_0), \tag{10}$$

where the front position $z_0(t)$ is promoted to a function of time, which we assume it satisfies $\dot{z}_0 \sim \gamma/k^3$. $w(z, z_0)$ is a small correction function ($w \ll 1$) which carry out $w \sim \gamma/k^3$. Introducing the ansatz (10) in Eq. (8), linearizing in w and applying a solvability condition, after straightforward calculation, we obtain

$$\dot{z}_0 = \Gamma + A\sin(kz_0 + \theta), \tag{11}$$

where $\Gamma \equiv -\sqrt{4/3}\Delta\mu + \beta/2\sqrt{3}\alpha^3, \theta \equiv \arctan(25/[36\alpha^3 - 75/2])$, and $A = \pi k^3/[72\alpha^6\sinh(2k\pi/\sqrt{3})(1296\alpha^6 - 2700\alpha^3 + 1875)^{1/2}]$.

A detailed analysis of the method to obtain the above equation is presented in Ref. 34. Therefore, the front position fulfills the dynamics of a particle in a washing board potential.[34] Namely, for $\Gamma/A < 1$, the front position has a family of stationary equilibria, separated by one or more wavelengths. This parameter region describes the pinning region. When $\Gamma/A > 1$, the front begins to propagate in a way that its speed is oscillatory, hopping dynamics. Analytically, one can determine the expression for the average speed $\langle\dot{z}_o\rangle$, which reads[41]

$$\langle\dot{z}_o\rangle = \begin{cases} \sqrt{\Gamma^2 - A^2}, & |\Gamma/A| > 1, \\ 0, & |\Gamma/A| < 1. \end{cases} \tag{12}$$

Then, in the pinning region, the front does not move. Outside this region, as μ increases, the speed grows with the square root ($\langle\dot{z}_o\rangle \propto \sqrt{\Gamma - A}$) and then grows linearly ($\langle\dot{z}_o\rangle \propto \Gamma - A$). Therefore, this model allows us to understand the numerical observations shown in Fig. 2.

In brief, the amended model in the high-frequency limit reveals how the equilibria are organized and the front features between these states. In Sec. IV, based on liquid crystal light valve with modulated optical forcing, the equilibria organization and the front connecting them will be experimentally studied.

IV. EXPERIMENTAL DESCRIPTION AND RESULTS

Liquid Crystal Light Valve (LCLV) with optical feedback is an experiment that exhibits a subcritical transition of molecular reorientation.[10] The LCLV corresponds to a nematic liquid crystal cell between a glass and a photoconductor plate. Both plates are coated with transparent electrodes (ITO), which allow applying an external electric field V_0 across the liquid crystal cell. Likewise, a dielectric mirror is deposed over the photoconductor plate. The light valve has a thickness of $d = 15\,\mu$m and planar alignment. The liquid crystal used in the cell is a nematic LC-654 (NIOPIK) and has a positive dielectric anisotropy $\epsilon_a = 10.7$. A He–Ne laser ($\lambda = 632.8$ nm) is used as the optical injection for the LCLV. To manipulate the profile (uniform or modulated) and intensity of the light, the input beam is sent through a spatial light modulator (SLM). The light reaching the LCLV will experience a change in its phase, if the effective voltage applied is above the transition threshold, V_T. Above this threshold, the liquid crystal molecules, in average, are reoriented to be aligned with the electric field. This molecular reorientation modifies the refractive index in the material. Hence, the light crossing and then reflecting on the dielectric mirror of the LCLV will experience a change in its phase related to the molecular orientation on the valve.[42] The optical feedback in the experiment is accomplished using an optical Fiber Bundle (FB) to guide the reflected beam to the photoconductor plate on the back of the LCLV. Depending on the illumination distribution on the photoconductor, the molecular orientation will change locally and dynamically. Part of the laser beam is sent to a charge-coupled device (CCD) camera, where the light reflected by the liquid crystal light valve, I_w, is monitored. Figure 4(a)

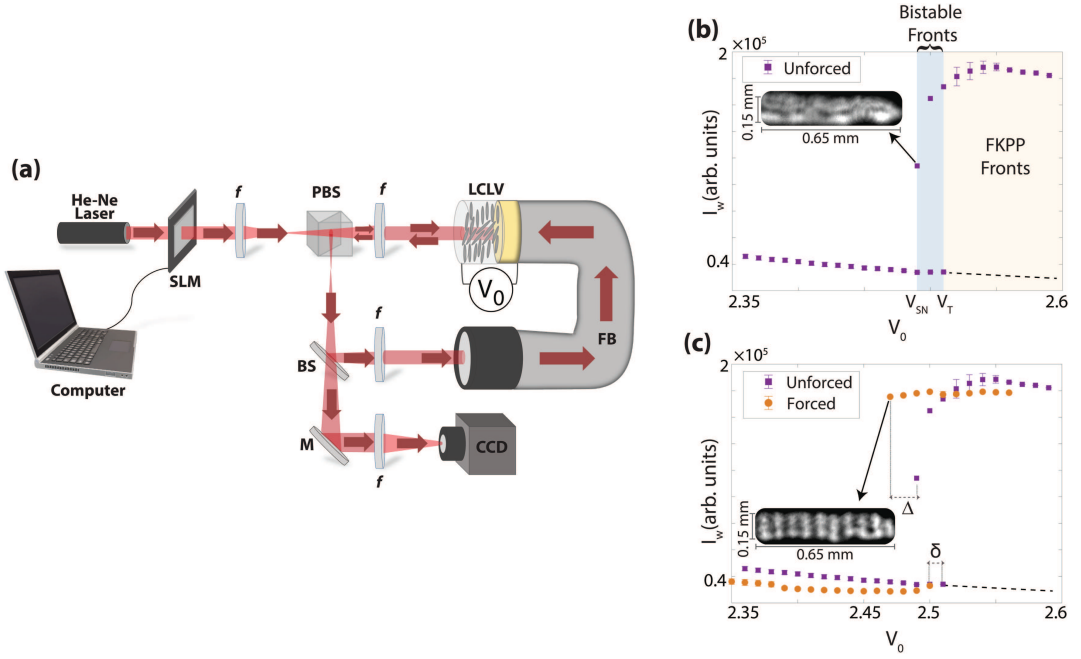

FIG. 4. Liquid crystal light valve (*LCLV*) without and with modulated optical forcing. (a) Schematic representation of the LCLV setup with optical feedback. *SLM* is the spatial light modulator, *PBS* is the polarized beam splitter, *BS* is the beam splitter, *M* is a mirror, *FB* is the fiber bundle, V_0 is the external voltage applied, *f* are lenses, and *CCD* is the camera that captures and records images. The LCLV is illuminated by a He–Ne laser. (b) Experimental bifurcation diagram obtained in the LCLV with uniform optical forcing, the unforced system. The total light intensity I_w at the LCLV is plotted as a function of the applied voltage V_0. The purple squares account for the experimental observations. The dashed line is a schematic representation of the unstable planar state. The inset corresponds to the typical observed reoriented state. Left and right painted areas show the bistability and monostable regions, respectively. The bistability region is characterized by $V_{SN} < V_0 < V_T$. (c) Experimental bifurcation diagram for the forced and unforced case, represented by orange dots and purple squares, respectively. δ and Δ stand for the displacement of the transition and bistable point, respectively. The inset corresponds to the typical reoriented pattern state in the forced system.

shows a schematic representation of the liquid crystal light valve with optical feedback. Experimental studies are performed at room temperature (26 °C).

The LCLV is illuminated with a quasi-one-dimensional channel (2.4 mm long by 0.24 mm wide) with homogeneous distribution of light (unforced case), using the SLM. The input light power reaching the LCLV was fixed at $I_{in} = 18\,\mu$W. We use the voltage V_0 applied to the optical valve as a control parameter. Figure 4(b) shows the experimental transition for the LCLV with uniform optical injection. The light intensity reflected by the light valve I_w exhibits a transition from a dark state (planar) to a bright state (reoriented). In the diagram, a hysteresis region is observed, where the planar and reoriented states coexist [intermediate painted region in Fig. 4(b)]. The limits of this region are characterized by $V_{SN} < V_0 < V_T$, which correspond to the bistability and transition voltage, respectively. In this region, fronts between these states can be found. Figure 5(a) shows the typical profile and spatiotemporal evolution of the fronts observed in this bistability region. Note that the front spreads with a constant speed, considering experimental imperfections. The experimental protocol to observe these fronts is based on the fact that initially the system is prepared onto a homogeneous state. Using the spatial light modulator, we generate a local disturbance, which induces the reoriented state to extend or contract. This propagation can be monitored through the CCD camera. The speed is measured tracking the interface between dark and bright areas. Figure 6(a) summarizes the experimental front speed. Note that the front speed increases as a function of the applied voltage. Besides, the Maxwell point is close to the left flank of the bistability region. Indeed, the experimental observations are in good agreement with those obtained by unforced model equation (1) [cf. Figs. 1, 4(b), and 5(a)].

Using the spatial light modulator, we can generate a spatial modulated input light with intensity, $I_{in}(x) = I_{in} + I_a \cos(kx)$, where I_a and k are the strength and the wavenumber of the forcing, respectively. Illuminating the LCLV, for sufficiently small voltage V_0, no significant changes are observed, the planar (dark) state remains stable. As the voltage increases, a discontinuous transition to a spatially modulated reoriented state begins to appear [see the inset in Fig. 4(c)]. In comparison to the unforced case, we observe that this reorientation transition is anticipated. Likewise, we observe that the bistability region moves to the left flank. Figure 4(c) shows the bifurcation diagram. Similar bifurcation diagram is obtained from the

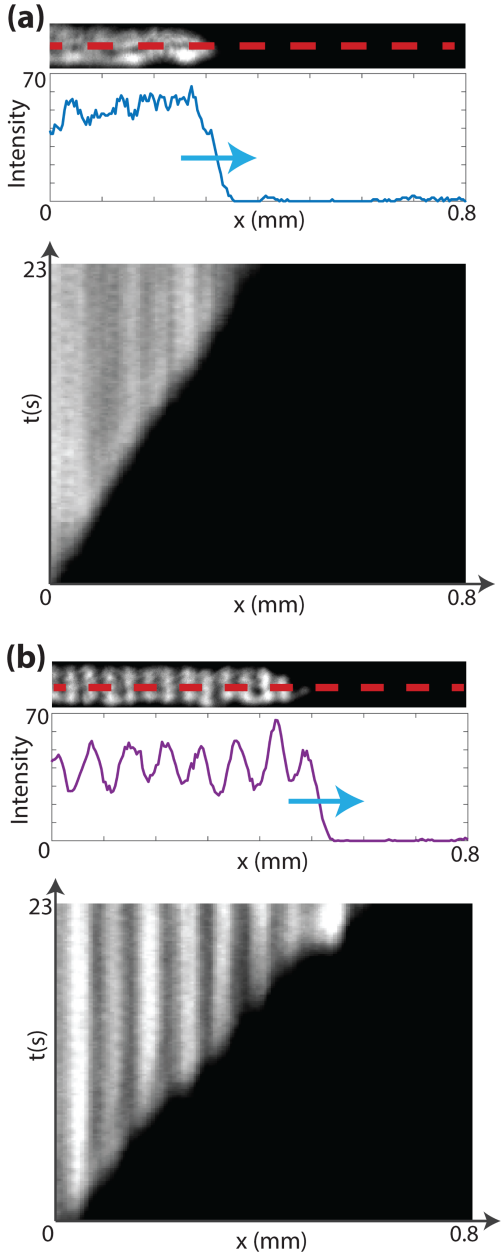

FIG. 5. Experimental front propagation in a LCLV with uniform and modulated optical forcing. (a) Panels account for a snapshot, profile, and spatiotemporal evolution of the front in the unforced case. The illuminated region corresponds to the reoriented state, and the dark region corresponds to the planar one. The dashed red curve is the extracted region to obtain its profile and spatiotemporal evolution. (b) Panels account for a snapshot, profile, and spatiotemporal evolution of the front in the forced case. The modulated reoriented state is observed as a pattern due to the forcing. The dashed red curve is the extracted region to obtain its profile and spatiotemporal evolution.

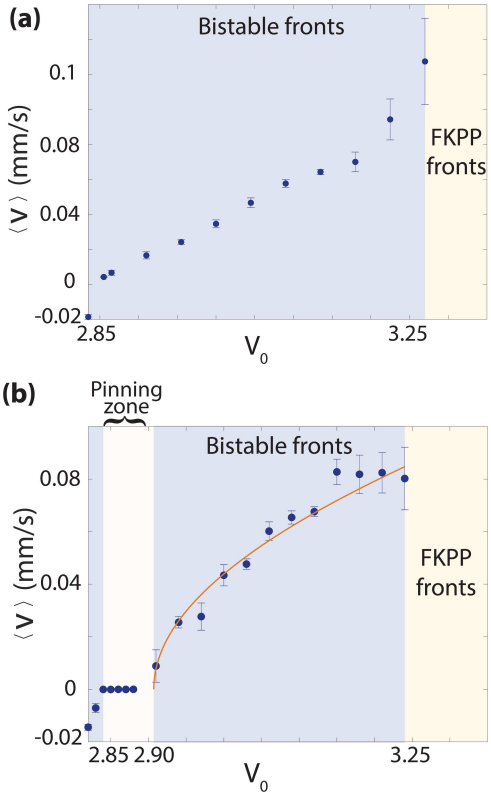

FIG. 6. Experimental average front speed of the liquid crystal light valve with a uniform and modulated optical forcing. Average front speed as a function of the applied voltage V_0 with uniform (a) and modulated (b) optical forcing. The color painting regions account for bistable, pinning, and coexistence region. Continuous curve is a fitting curve using formula (12).

forced model equation (1) [cf. Fig. 2]. With the same strategy, fronts connecting a planar state with the reoriented modulated state can be generated. Figure 5(b) shows the typical profile and spatiotemporal evolution of these fronts. The evolution of the front is characterized by exhibiting a hopping dynamic. Figure 6(b) displays the average front speed as a function of the applied voltage V_0. As one expects, at low applied voltages, the planar state invades the spatially modulated reoriented state. As the voltage increases, one observes that the front becomes motionless in a large region of the space of parameters, often called the pinning region. Out of this regime, one expects that the modulated state invades the planar state. The front speed in this region must be characterized by a square root of the difference of squares, formula (12). In Fig. 6, this type of fitting is used to characterize the average speed, see the continuous curve. Hence, the theoretical findings have excellent agreement with the experimental observations.

One of the main results of the high-frequency theory is that the critical transition point is modified with the inverse of the square of the wavenumber. Experimentally, for different wavenumber of

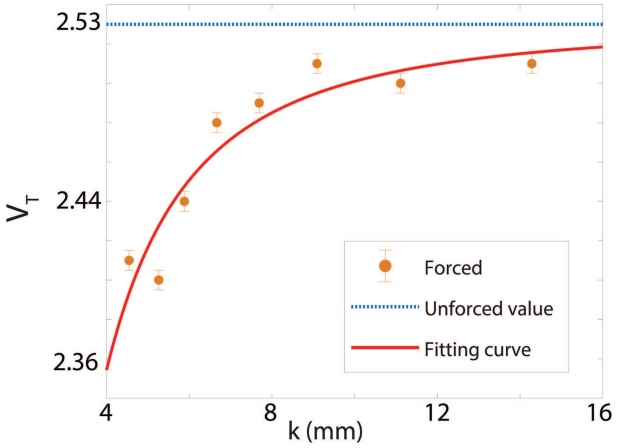

FIG. 7. Experimental modification of the critical transition voltage V_T as a function of the forcing wavenumber k. The orange dots correspond to the forced case with different values of k and fixed value of forcing amplitude at $I_a = 4\ \mu$W. The dashed blue line is the value for the transition voltage in the unforced case. The solid red line corresponds to a fitting curve $V_T = -H/k^2 + c$ with $H = 2.7$ and $c = 2.53$.

the optical forcing, the critical voltage for the reorientation transition has been measured. Figure 7 summarizes the results found. From these observations, we can conclude that the critical voltage V_T decreases with the inverse of the square of the forcing wavenumber.

V. CONCLUSION

Driven systems with temporal and spatial forcing present complex spatiotemporal behaviors. An analytical strategy to achieve a better understanding of these systems is to consider extreme limits of parameters to obtain effective models. This strategy is what we have used to understand spatially modulated systems. That is, we have taken the limit of high-wavenumber forcing, the homogenization method. This method allows us to transform a spatially modulated system into an effective homogeneous system with renormalized parameters. In this context, it is more feasible to obtain analytical results. Based on an amplitude equation that describes the reorientation transition of a liquid crystal light valve with spatially modulated optical forcing and the homogenization method, we have characterized the organization of the equilibria. In particular, we have shown that the forcing induces patterns that coexist with the uniform state in regions where the system without forcing is monostable. We have analytically identified how the bistability region moves and verified this prediction experimentally, finding excellent agreement. However, the homogenized amplitude equation does not account for the front dynamics. This is because, in this limit, the interaction between the front core dynamics and the rapid oscillation is decoupled. To address this dynamic, we have amended the amplitude equation, that is, we have taken into account the first corrective terms in the homogenization method. Using perturbative theory, these terms allow us to describe the experimentally observed dynamics.

Systems under spatiotemporal forcing exhibit complex behaviors. A strategy to better understand spatially modulated forced systems could be led with a high-wavelength limit. Work in this direction is in progress.

ACKNOWLEDGMENTS

The authors acknowledge financial support from the Millennium Institute for Research in Optics. M.G.C. acknowledges FONDECYT Project No. 1180903. G.G. acknowledges financial support from CONICYT by Doctorado Nacional No. 2017-21171672. This work is dedicated to the late Professor Enrique Tirapegui (1940–2020).

DATA AVAILABILITY

The data that support the findings of this study are available from the corresponding author upon reasonable request.

REFERENCES

[1] P. Glansdorff and I. Prigogine, *Thermodynamic Theory of Structures, Stability and Fluctuations* (Wiley, New York, 1971).
[2] G. Nicolis and I. Prigogine, *Self-Organization in Nonequilibrium Systems* (Wiley & Sons, New York, 1977).
[3] M. C. Cross and P. C. Hohenberg, "Pattern formation outside of equilibrium," Rev. Mod. Phys. **65**, 851 (1993).
[4] L. M. Pismen, *Patterns and Interfaces in Dissipative Dynamics* (Springer, Berlin, 2006).
[5] J. S. Langer, Rev. Mod. Phys. **52**, 1 (1980).
[6] Y. Pomeau, Physica D **23**, 3 (1986).
[7] P. Collet and J. P. Eckmann, *Instabilities and Fronts in Extended Systems* (Princeton University Press, Princeton, 1990).
[8] J. D. Murray, *Mathematical Biology* (Springer-Verlag, Berlin, 1993).
[9] C. Chevallard, M. G. Clerc, P. Coullet, and J. M. Gilli, Eur. Phys. J. E **1**, 179 (2000).
[10] M. G. Clerc, S. Residori, and C. Riera, Phys. Rev. E **63**, 060701 (2001).
[11] W. van Saarloos, Phys. Rep. **386**, 29 (2003).
[12] S. Residori, A. Petrossian, T. Nagaya, C. Riera, and M. G. Clerc, Physica D **199**, 149 (2004).
[13] A. Hubert and R. Schafer, *Magnetic Domains: The Analysis of Magnetic Microstructures* (Springer Science & Business Media, Berlin, 2008).
[14] F. Haudin, R. G. Elías, R. G. Rojas, U. Bortolozzo, M. G. Clerc, and S. Residori, Phys. Rev. Lett. **103**, 128003 (2009); F. Haudin, R. G. Elías, R. G. Rojas, U. Bortolozzo, M. G. Clerc, and S. Residori Phys. Rev. E. **81**, 056203 (2010).
[15] V. Mendez, S. Fedotov, and W. Horsthemke, *Reaction-Transport Systems: Mesoscopic Foundations, Fronts, and Spatial Instabilities* (Springer Science & Business Media, Berlin, 2010).
[16] E. Macias, M. G. Clerc, C. Falcon, and M. A. Garcia-Nustes, Phys. Rev. E **88**, 020201(R) (2013).
[17] W. van Saarloos and P. C. Hohenberg, Physica D **56**, 303 (1992).
[18] C. Castillo-Pinto, M. G. Clerc, and G. González-Cortés, Sci. Rep. **9**, 15096 (2019).
[19] A. J. Alvarez-Socorro, M. G. Clerc, G. González-Cortés, and M. Wilson, Phys. Rev. E **95**, 010202(R) (2017).
[20] P. Coullet, J. Lega, B. Houchmanzadeh, and J. Lajzerowicz, Phys. Rev. Lett. **65**, 1352 (1990).
[21] D. Michaelis, U. Peschel, F. Lederer, D. V. Skryabin, and W. J. Firth, Phys. Rev. E **63**, 066602 (2001).
[22] M. G. Clerc, S. Coulibaly, and D. Laroze, Int. J. Bifurcat. Chaos **19**, 2717 (2009).
[23] R. A. Fisher, Ann. Eugenics **7**, 355 (1937).

[24]A. Kolmogorov, I. Petrovsky, and N. Piscounov, Bull. Univ. Moscow Ser. Int. A **1**, 1 (1937).
[25]G. Ahlers and D. S. Cannell, Phys. Rev. Lett. **50**, 1583 (1983).
[26]J. Fineberg and V. Steinberg, Phys. Rev. Lett. **58**, 1332 (1987).
[27]J. Langer, *An Introduction to the Kinetics of First-Order Phase Transition, Solids Far from Equilibrium* (Cambridge University Press, Cambridge, 1992).
[28]M. G. Clerc, T. Nagaya, A. Petrossian, S. Residori, and C. S. Riera, Eur. Phys. J. D **28**, 435 (2004).
[29]K. Alfaro-Bittner, C. Castillo-Pinto, M. G. Clerc, G. González-Cortés, R. G. Rojas, and M. Wilson, Phys. Rev. E **98**, 050201(R) (2018).
[30]A. J. Alvarez-Socorro, C. Castillo-Pinto, M. G. Clerc, G. González-Cortés, and M. Wilson, Opt. Express **27**, 12391 (2019).
[31]S. Coen, M. Tlidi, Ph. Emplit, and M. Haelterman, Phys. Rev. Lett. **83**, 2328 (1999).
[32]V. Odent, M. Tlidi, M. G. Clerc, P. Glorieux, and E. Louvergneaux, Phys. Rev. A **90**, 011806(R) (2014).
[33]M. G. Clerc, S. Coulibaly, and M. Tlidi, Phys. Rev. Res. **2**, 013024 (2020).
[34]M. G. Clerc, C. Falcon, and E. Tirapegui, Phys. Rev. Lett. **94**, 148302 (2005); M. G. Clerc, C. Falcon, and E. Tirapegui Phys. Rev. E **74**, 011303 (2006).
[35]F. Marino, G. Giacomelli, and S. Barland, Phys. Rev. Lett. **112**, 103901 (2014).
[36]E. Sánchez-Palencia, *Nonhomogeneous Media and Vibration Theory*, Notes in Physics (Springer-Verlag, Berlin, 1980).
[37]N. Bakhvalov and G. Panasenko, *Homogenisation: Averaging Processes in Periodic Media* (Kluwer Academic Publishers Group, Dordrecht, 1989).
[38]C. C. Mei and B. Vernescu, *Homogenization Methods for Multiscale Mechanics* (World Scientific, 2010).
[39]G. Pavliotis and A. Stuart, *Multiscale Methods: Averaging and Homogenization* (Springer Science & Business Media, New York, 2008).
[40]C. M. Bender and S. A. Orszag, *Advanced Mathematical Methods for Scientists and Engineers I: Asymptotic Methods and Perturbation Theory* (Springer Science & Business Media, New York, 1999).
[41]R. G. Rojas, "Sur de gouttes, cristaux liquides et fronts," dissertation (University of Nice Sophia Antipolis, 2005), see http://tel.archives- ouvertes.fr.
[42]S. Residori, Phys. Rep. **416**, 201 (2005).